Mutations in *FBXL4* Cause Mitochondrial Encephalopathy and a Disorder of Mitochondrial DNA Maintenance

Penelope E. Bonnen,[1,2,*] John W. Yarham,[3] Arnaud Besse,[1,2] Ping Wu,[1] Eissa A. Faqeih,[4] Ali Mohammad Al-Asmari,[4] Mohammad A.M. Saleh,[4] Wafaa Eyaid,[5] Alrukban Hadeel,[5] Langping He,[3] Frances Smith,[6] Shu Yau,[6] Eve M. Simcox,[3] Satomi Miwa,[7] Taraka Donti,[1] Khaled K. Abu-Amero,[8] Lee-Jun Wong,[1] William J. Craigen,[1] Brett H. Graham,[1] Kenneth L. Scott,[1] Robert McFarland,[3] and Robert W. Taylor[3,*]

Nuclear genetic disorders causing mitochondrial DNA (mtDNA) depletion are clinically and genetically heterogeneous, and the molecular etiology remains undiagnosed in the majority of cases. Through whole-exome sequencing, we identified recessive nonsense and splicing mutations in *FBXL4* segregating in three unrelated consanguineous kindreds in which affected children present with a fatal encephalopathy, lactic acidosis, and severe mtDNA depletion in muscle. We show that FBXL4 is an F-box protein that colocalizes with mitochondria and that loss-of-function and splice mutations in this protein result in a severe respiratory chain deficiency, loss of mitochondrial membrane potential, and a disturbance of the dynamic mitochondrial network and nucleoid distribution in fibroblasts from affected individuals. Expression of the wild-type *FBXL4* transcript in cell lines from two subjects fully rescued the levels of mtDNA copy number, leading to a correction of the mitochondrial biochemical deficit. Together our data demonstrate that mutations in *FBXL4* are disease causing and establish FBXL4 as a mitochondrial protein with a possible role in maintaining mtDNA integrity and stability.

Introduction

Pediatric-onset mitochondrial disease has an estimated incidence of 1 in 5,000,[1] but despite this common occurrence the molecular etiology in individual cases often remains unknown. Mitochondria play a key role in a variety of fundamental cellular processes including oxidative phosphorylation (OXPHOS), essential metabolic pathways, apoptosis, and calcium buffering. Mitochondria have a unique bigenomic heritage, and their proper functioning is consequently dependent upon the coordinated expression and interaction of both nuclear and mitochondrial-encoded gene products.[2] More than 1,000 nuclear genes play a role in mitochondrial function,[3] giving rise to a potential for extensive genetic heterogeneity in the primary mitochondrial disease population. Most cases are therefore probably caused by nuclear-encoded mutations, with autosomal-recessive transmission being most commonly observed.[1,4] Clinical presentation varies widely and can involve multiple organ systems, often triggering extensive diagnostic investigations that result in a molecular diagnosis for a minority of individuals.

Mutations have been described in a number of nuclear genes involved in the maintenance of mitochondrial DNA (mtDNA), ultimately leading to secondary mtDNA abnormalities in clinically affected tissues. Damage to mtDNA manifests in two molecularly distinct forms: the accumulation of clonally expanded mtDNA deletions associated with focal respiratory-deficient cells and a quantitative loss of mtDNA copy number that is characteristic of mtDNA depletion syndromes. Multiple mtDNA deletion disorders typically manifest in adulthood,[5] whereas mtDNA depletion disorders are usually very severe, early-onset diseases of childhood characterized by isolated organ or multisystem involvement.[6] With the exception of MPV17 whose function remains unknown,[7] the products of identified candidate genes are involved in either mtDNA replication/repair or the maintenance of mitochondrial deoxyribonucleotide pools required for faithful mtDNA synthesis.[1,3]

Here, we report the finding of mutations in *FBXL4* (MIM 605654), which encodes an orphan F-box protein, identified in affected children from three unrelated families with multiple mitochondrial respiratory chain defects and mtDNA depletion. Moreover, we provide evidence that mutations in this gene cause defective mtDNA maintenance resulting in extensive mitochondrial dysfunction leading to severe encephalopathy.

[1]Department of Molecular and Human Genetics, Baylor College of Medicine, Houston, TX 77030, USA; [2]Human Genome Sequencing Center, Baylor College of Medicine, Houston, TX 77030, USA; [3]Wellcome Trust Centre for Mitochondrial Research, The Medical School, Newcastle University, Newcastle upon Tyne NE2 4HH, UK; [4]Section of Medical Genetics, Children's Hospital, King Fahad Medical City, P.O. Box 59046, Riyadh 11525, Saudi Arabia; [5]Department of Pediatrics, King Abdulaziz Medical City, King Saud Bin Abdulaziz University for Health & Science, P.O. Box 22490, Riyadh 11426, Saudi Arabia; [6]DNA Laboratory, Guy's and St Thomas' Serco Pathology, Guy's Hospital, London SE1 9RT, UK; [7]Institute for Ageing and Health, Newcastle University, Newcastle upon Tyne NE4 5PL, UK; [8]Ophthalmic Genetics Laboratory, Department of Ophthalmology, College of Medicine, King Saud University, P.O. Box 245, Riyadh 11411, Saudi Arabia
*Correspondence: pbonnen@bcm.edu (P.E.B.), robert.taylor@ncl.ac.uk (R.W.T.)
http://dx.doi.org/10.1016/j.ajhg.2013.07.017.

Material and Methods

Subjects

Informed consent for diagnostic and research studies was obtained for all subjects or their parents and for 204 healthy, ethnically matched anonymized Arabian controls in accordance with the Declaration of Helsinki protocols and approved by local Institutional Review Boards. Genomic DNA was extracted from peripheral-blood lymphocytes, skeletal muscle, fibroblasts, and/or saliva according to standard protocols.

Muscle Histology and Respiratory Chain Activity Assays

Routine histological staining and histochemical reactions of oxidative enzyme activities including cytochrome *c* oxidase (COX) were performed on fresh-frozen sections (10 μm) of muscle according to established protocols.[8] The activities of the individual respiratory chain complexes I–IV were measured in skeletal muscle homogenates and cultured fibroblasts as described previously[9] and activities expressed relative to that of citrate synthase (a matrix marker enzyme) for the muscle, or relative to mitochondrial protein for the cells, and expressed as a percentage of normal controls.

Identification and Validation of Pathogenic *FBXL4* Mutations

Initial molecular studies involved the exclusion of large-scale mtDNA rearrangements by long-range PCR,[10] sequencing of the entire mitochondrial genome (ABI 3130xl, Applied Biosystems) essentially as described,[11,12] and the assessment of mtDNA copy number in muscle.[13]

Exonic sequences were targeted and enriched from genomic DNA with the Agilent SureSelect Human exome kit (subject 1 [S1]) and sequenced on an Illumina Genome Analyzer IIx. Whole-exome sequencing was conducted on subject 2 (S2) and subject 3 (S3) with a custom capture design called "VCROME" developed at the BCM Human Genome Sequencing Center that enriches for approximately 20,000 genes comprising a total of 45 Mb of captured genomic sequence.[14] Samples were sequenced in a paired-end strategy on an Illumina HiSeq 2000 instrument.

Sequence data alignments were performed to human reference sequence hg19 (UCSC Genome Browser) by BWA software.[15] Duplicate reads were removed with the Picard program. Recalibration and realignment of the data were accomplished with the Genome Analysis Toolkit (GATK).[16,17] Single-nucleotide variants (SNVs) and small insertions and deletions (indels) were called by GATK. Quality control filtering of variants was based on coverage, strand bias, mapping quality, and base quality. Annotation of variants was conducted with internally developed Perl scripts. Prediction for potential functional consequences of variants was conducted with SIFT[18] and PolyPhen2.[19] The evolutionary conservation of missense mutations was determined by genomic evolutionary rate profiling (GERP), which approximates evolutionary constraint at a locus by maximum likelihood estimation,[20,21] and PhyloP, which predicts departures from the neutral evolution,[22] and the reported score is the result of analysis of an alignment of 46 different placental mammal species. The range of scores is from −13.9 (minimum) to 2.9 (maximum) with mean = 0.03. The GERP++ score reported here is based on the alignment of 35 mammalian species and the maximum GERP score for this analysis is 6.18.

Orthogonal validation of *FBXL4* mutations was completed for each propositus, and recessive segregation was confirmed with PCR-based Sanger sequencing with the following primer pairs (*FBXL4* GenBank accession number NM_012160.3): S1_Fwd 5′-TGTAAAACGACGGCCAGTAACAGTTTGCATGTCTGAGCA-3′ and S1_Rev 5′-CAGGAAACAGCTATGACCAAACCAAGCCATCT TATCAGGA-3′; S2_Fwd 5′-GCTTACCTCAACCAACGCTTA-3′ and S2_Rev 5′-GCCTTGAATTGTCTTGCAGC-3′; and S3_Fwd 5′-CTGCGAACAGAAGGACACATC-3′ and S3_Rev 5′-GTCCTAGAT GCTAAATTGGCTGG-3′. Each of the *FBXL4* mutations was further investigated in 204 ethnically matched healthy Arab controls by direct Sanger sequencing across the mutation site.

Determination of mtDNA Copy Number in Tissues

In addition to testing muscle mtDNA copy number,[13] this was also determined in cultured fibroblasts by real-time qPCR essentially as described previously[23,24] with beta-2 microglobulin (*B2M*) as the nuclear gene (nDNA) normalizer for the calculation of mtDNA/nDNA ratio. The *ND1* region of human mtDNA was amplified with forward primer 5′-GTCAACCTCGCTTCCCCACCCT-3′ and reverse primer 5′-TCCTGCGAATAGGCTTCCGGCT-3′. A fragment of human *B2M* was amplified with forward primer 5′-CGACGG GAGGGTCGGGACAA-3′ and reverse primer 5′-GCCCCGCGAAA GAGCGGAAG-3′. The PCR reaction was conducted (in triplicate) on total genomic DNA and utilized iTaqTM SYBR Green Supermix with ROX (Bio-Rad Laboratories).

qRT-PCR

RNA was extracted from confluent cells with TRIzol reagent (Life Technologies) according to manufacturer instructions, treated with RQ1 RNase-free DNase, and purified with PureLink RNA mini kit (Life Technologies). Synthesis of cDNA was performed with SuperScript III (Life Technologies) and oligodT according to manufacturer instructions. Quantitative real-time PCR experiments were performed with a StepOne Plus RT-PCR system (Applied Biosystems), RT2 qPCR Primer Assays for Human *GAPDH* and *FBXL4* (SABiosciences), and PerfeCTa SYBR Green FastMix ROX (Quanta Biosciences).

Oligodeoxynucleotide primers and dual-labeled probes to detect either spliced or unspliced forms of *FBXL4* were as follows: *FBXL4*-unspliced_Fwd, 5′-GCAGTGTCACAGTAGTTA-3′; *FBXL4*-unspliced_Rev, 5′-ACCTGAATCTTGCCAATA-3′; *FBXL4*-unspliced_Probe, 5′-CCACTATCTTCATTCCTACCTCCTACC-3′; *FBXL4*-spliced_Fwd, 5′-GACACAGACATTGATGAA-3′; *FBXL4*-spliced_Rev, 5′-GGAG TTTTCTTAAGGATGC-3′; and *FBXL4*-spliced_Probe, 5′-ACCATTC TTGTTCCTAATATGTCCAGC-3′. The cycle of threshold value (Ct) was normalized to the transcripts for the housekeeping gene *GAPDH*. All assays were conducted in triplicate and the results are shown as the average and standard deviation.

Bioinformatic Analysis of the FBXL4 Protein

Protein structure modeling was conducted with the Phyre2 server with the 3D structure image realized by JMOL.[25] Mitochondrial localization signal prediction was determined with MitoProt.[26] Conserved domains were determined with NCBI Conserved Domain Database (CDD).[27]

Fibroblast Cell Culture

Fibroblasts from two affected individuals (S1 and S2) and age-matched controls were grown in MEM (Life Technologies) supplemented with FBS to 10%, 1× MEM vitamins, 2 mM L-glutamine,

1 mM sodium pyruvate, 1× penicillin/streptomycin, 1× nonessential amino acids, and 0.41 μM uridine. Cells were maintained as a monolayer in a humidified 37°C, 5% CO_2 atmosphere.

Investigation of Mitochondrial and Nucleoid Morphology

Fibroblasts were grown in 35 mm imaging dishes (iBIDI, Thistle Scientific) to 70%–80% confluency. Cells were incubated at 37°C in the growth media described above, supplemented with either 3 μl of PicoGreen (Invitrogen) for 45 min or with 100 nM MitoTracker Red (Invitrogen) for 25 min. Cells were washed in standard media and imaging performed with a 63× oil immersion lens on the inverted Axiovert 200M (Zeiss), with shutter speeds of 200 ms and 75 ms for MitoTracker Red and PicoGreen, respectively.

Assessment of Mitochondrial Membrane Potential

Mitochondrial membrane potential was assessed with MitoProbe DilC1(5) Assay kit for Flow Cytometry (Life Technologies) following general manufacturer recommendations with some modifications. In brief, confluent cells were harvested and counted with Vi-CELL cell viability analyzer (Beckman Coulter). The cells were either stained directly with 50 nM DilC1(5) dye for 30 min at 37°C, 5% CO_2, or preincubated with 50 mM carbonyl cyanide 3-chlorophenylhydrazone (CCCP) for 15 min at 37°C, 5% CO_2 prior to staining with DilC1(5). Cells were analyzed on a flow cytometer with 633 nm excitation. Results are reported as the difference between the mean fluorescence intensity (MFI) of cells treated with CCCP or not. All assays were conducted in triplicate and shown as the average and standard deviation.

Microscale Oxygraphy Analysis

Mitochondrial respiratory activity was measured in live fibroblasts by microscale oxygraphy analysis with the Seahorse Biosciences XF24 Analyzer (Seahorse Biosciences). Cells were seeded onto 24-well plates at a density of 30,000 cells/well and prior to performing the experiment, the growth media was replaced with basic media supplemented with FBS to 3%, 10 mM pyruvate, 2 mM L-glutamine, and 1 mg/ml glucose and the cells incubated in a CO_2-free atmosphere. Measurements of O_2 consumption rate (OCR) and proton production rate (PPR) were taken at regular intervals while the following compounds were injected to test mitochondrial activity: oligomycin (to 1.3 μM) to block the ATP synthase, two sequential additions of carbonyl cyanide p-trifluoromethoxy-phenylhydrazone (FCCP), a respiratory chain uncoupler to drive maximum respiratory capacity (first to 2 μM, then to 3 μM), and antimycin (to 2.5 μM), which blocks Complex III.[28]

Data were normalized by cell number, and a number of parameters assessed,[29] subsequent to the subtraction of nonmitochondrial respiration (NMR) from each value. ATP production by OXPHOS was calculated by multiplying ATP turnover ((basal OCR – NMR) – (oligomycin-inhibited OCR – NMR)) by the established phosphorus/oxygen (P/O) ratio of 2.3.[30] ATP production by glycolysis is considered to have a 1:1 ratio with lactate production, which is measured by PPR.[31] Spare respiratory capacity = ((maximal OCR – NMR) – (basal OCR – NMR)), whereas ATP coupling efficiency = ((basal OCR – NMR) – (oligmycin-inhibited OCR)) / basal OCR × 100). Five separate control cell lines underwent multiple testing ($n \geq 10$) and the means were combined to calculate control data (mean ± SD; $n = 5$). Cell lines from each subject were also tested multiple times ($n \geq 10$). An unpaired, two-tailed Student's t test was performed to determine the significance of any differences between the data sets and p values were considered significant at the 95% confidence interval.

Immunoblotting

Total cellular protein was extracted, size-separated on 12% gels by SDS-PAGE, and transferred to a methanol-activated PVDF membrane. Immunoblotting was performed with primary antibodies from Abcam (NDUFA9, NDUFB8, NDUFA13, SDHA, UQCRC2, MTCOI, MTCOII, COXIV, ATPB, and TOMM20) and Sigma (β-actin). Chemiluminescent detection of the bands was achieved with the Amersham ECL Prime Kit (GE Healthcare) for signal development, according to the manufacturer's instructions, and the membrane was viewed with the ChemiDocMP Imaging System (Bio-Rad).

Gene Rescue Studies

Fibroblasts from subjects and controls were stably infected with a pLX302 lentiviral mammalian expression vector system expressing *EGFP* and *FBXL4* cDNA (NM_012160.3). HEK293 cells were plated in DMEM (Hyclone) with 10% FBS (Atlanta Biologicals) and transfected with pLX302-EGFP/pLX302-FBXL4 in Opti-MEM medium I (Life Technologies) and the packaging mix (5 μg pMDLg/pRRE, 2.5 μg RSV-rev, and 3 μg MD2.VSVG) with Lipofectamine 2000 (Life Technologies). Infectious lentiviral supernatant was collected at 48 and 60 hr, filtered, and used to infect growing fibroblasts with 8 μg/ml polybrene (Sigma) before selection by puromycin (1.25 μg/ml).

Mitochondrial Localization Studies of the FBXL4 Protein

Healthy control fibroblasts were infected with pBabe vector containing HA-tagged *FBXL4* cDNA (NM_012160.3) and selected with puromycin (1.25 μg/ml). Noninfected cells and HA-*FBXL4*-expressing cells were seeded on a micro-Slide VI flat ibiTreat microscopy chamber (Ibidi) at 50%–60% confluence. Cells were incubated for 10 min in normal growth medium containing 100 nM MitoTracker Red CMXRos (Molecular Probes) and fixed with 4% paraformaldehyde. Cells were permeabilized by incubation in 0.1% Triton X-100 and blocked in 10% normal goat serum. Fluorescent staining was performed with mouse anti-HA primary antibody (Cell Signaling) and AlexaFluor 488 goat anti-mouse secondary antibody (Life Technologies). Cells were counterstained in Vectashield mounting medium with DAPI (Vector Laboratories) and visualized at 100× magnification with a Nikon Eclipse 90i microscope. The images were processed with NIS-elements v.3.0 software.

Results

Mutations in *FBXL4* Identified in Individuals with Encephalopathy and Persistent Lactic Acidosis

Detailed descriptions of the three families (all of Arabian origin) and affected cases studied are provided in Table 1. Subject 1 (S1) presented with delayed milestones and brain atrophy by CT at the age of 3 months, which worsened by 14 months to include severe psychomotor delay, poor growth, and persistent lactic acidosis. This individual died of encephalopathy at the age of 3 years, 9 months.

Table 1. Clinical Presentation of Affected Children from Three Families

Subject	Birth Weight (Gestation)	Dysmorphic Features	Microcephaly	Dev. Delay	Tone	Eye Disease	Cranial MRI	Lactic Acidosis		Elevated Blood Ammonia	Age at Death
								Y/N	Onset		
S1 (family 1, V-11)	1.5 kg (T)	none	congenital; <3rd centile	global	normal	no	generalized cerebral atrophy	Y	14 months	no	3 years 9 months
V-8 (family 1)	2.5 kg (T)	none	congenital; <3rd centile	global	low	no	normal	Y	birth	yes	1 year 8 months
V-3 (family 1)	2.3 kg (T)	yes (craniofacial)	acquired; <3rd centile at 2 years	global	low	congenital cataracts	dilated ventricles, hypoplastic left hemisphere and cerebellar vermis	Y	4 months	no	2 years
V-4 (family 1)	2.2 kg (T)	none	no	no	low	not checked	not done	Y	birth	yes	3 days
IV-5 (family 1)	unknown	unknown	unknown	yes	unknown	unknown	unknown	Y	birth	unknown	4 years
S2 (family 2)	2.3 kg (T)	yes (craniofacial)	no	global	low	cataracts, OA	abnormal dorsal brainstem and post limb of IC, prominent CM	Y	birth	no	4 months
S3 (family 3)	2.6 kg (T)	yes (craniofacial)	unknown	global	low	no	generalized atrophy, delayed myelination, abnormal signal in BG and brainstem	Y	6 years	unknown	alive at 6 years

Abbreviations are as follows: BG, basal ganglia; CM, cisterna magna; Dev delay, developmental delay; IC, internal capsule; OA, optic atrophy; T, term (>37 weeks <41 weeks).

The extended family of S1 is significant for consanguinity and includes four similarly affected children (Figure 1A, Table 1). In order to elucidate the molecular basis of this fatal encephalopathy and severe lactic acidosis, we performed whole-exome sequencing in S1 (Figure 1A, subject IV-11). Identified variants were prioritized as being likely disease-causing mutations by a recessive model of inheritance, population allele frequency of <0.001, and potential for damaging protein function and evolutionary conservation. We identified a potentially pathogenic truncating mutation (*FBXL4* c.1555C>T [p.Gln519*]) in *FBXL4* (GenBank accession number NM_012160.3), which encodes an F-box and leucine-rich repeat (LRR) protein. The homozygous c.1555C>T (p.Gln519*) mutation occurs in the C-terminal LRR domain, which provides substrate interaction and specificity for FBXL proteins (Figure 2A). This variant was not observed by the 1000 Genomes Project or the NHLBI Exome Sequencing Project. Importantly, it was shown to be absent from a panel of 408 ethnically matched control chromosomes. The c.1555C>T (p.Gln519*) mutation showed complete segregation with the disease phenotype in all clinically affected family members (Figure 1A: III-5, IV-3, IV-4, IV-8, and IV-11); all parents were heterozygous carriers and unaffected children available for genetic screening (Figure 1A: IV-1, IV-2, and IV-7) were either carriers or did not harbor the mutation.

Two additional, unrelated individuals presenting with similar symptoms early in life were subsequently subjected to whole-exome sequencing, revealing additional mutations in *FBXL4*. Subject 2 (S2) presented in the first month of life with severe hypotonia, encephalopathy, cardiomyopathy, and lactic acidosis (serum lactate 18 mmol/l; normal control range 0.7–2.1 mmol/l), leading to death at age 4 months (Table 1). Three older siblings presented with a similar fatal, early-onset phenotype, and the proband's mother has also suffered three miscarriages (Figure 1B). Exome sequencing revealed that S2 was homozygous for a different nonsense mutation in *FBXL4* (c.1303C>T [p.Arg435*]), predicting an earlier truncation of the protein than that observed in S1.

Subject 3 (S3) is a 6-year-old boy with a similar but less severe clinical presentation (Table 1). Born to consanguineous parents (Figure 1C), he has a history of severe intellectual disability, global developmental delay, hypotonia, poor growth, and persistent lactic acidosis. Imaging of the brain by magnetic resonance imaging (MRI) without contrast demonstrated global volume loss particularly the subcortical and periventricular white matter with significant abnormal signal in bilateral basal ganglia and brainstem with associated delayed myelination. Magnetic resonance spectroscopy of the brain demonstrated an elevated lactate peak. S3 is homozygous for a missense mutation (*FBXL4* c.1703G>C) in the first base of the last exon, which we demonstrated affects the splicing of this exon (Figure 2C).

The *FBXL4* mutations identified in S2 and S3 were also determined to be absent from 408 ethnically matched (Arabian) control chromosomes. Neither mutation was present in the 1000 Genomes Project database. The c.1303C>T (p.Arg435*) mutation found in S2 was

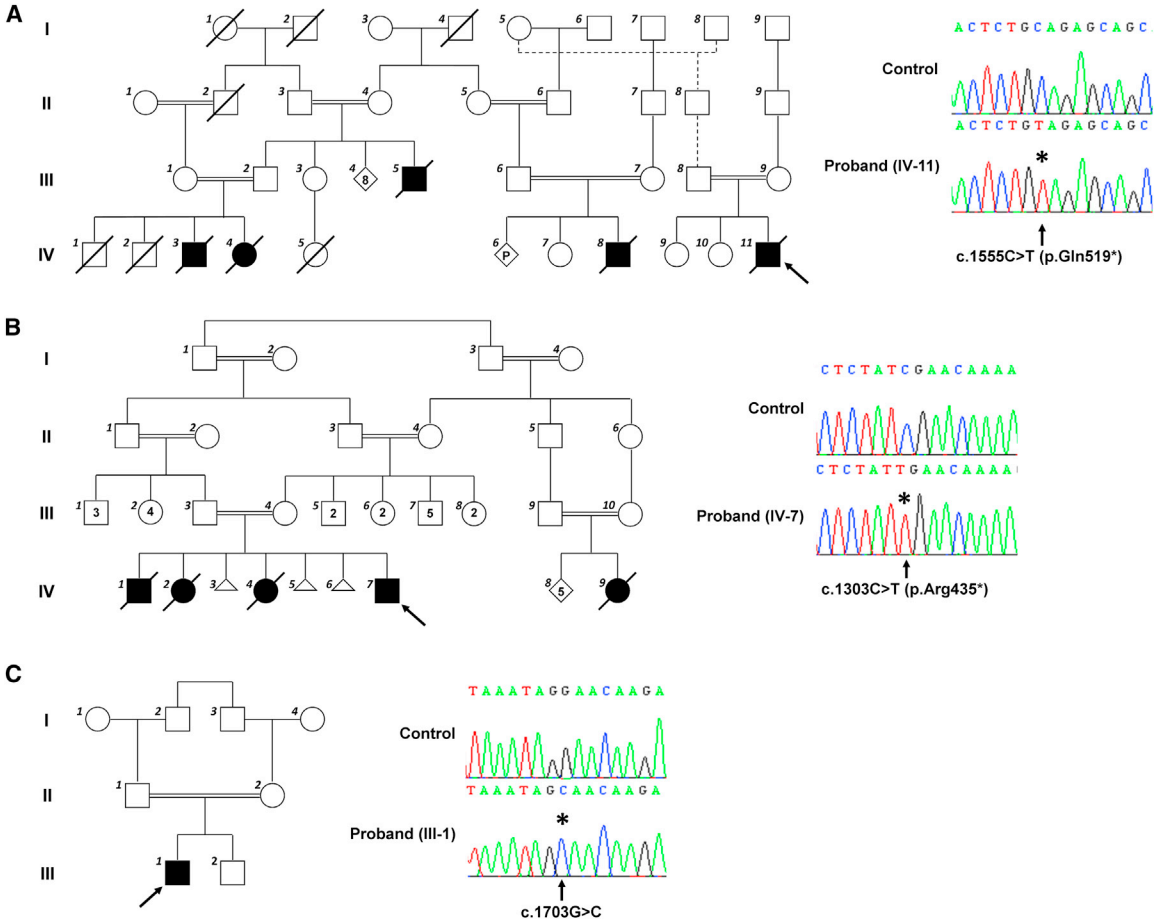

Figure 1. Genetic Investigation of the Families Confirms Segregation with Disease of Recessive *FBXL4* Mutations
The pedigrees of S1 (A), S2 (B), and S3 (C) are shown, highlighting the consanguineous nature of each family. The probands are indicated by black arrows, and all individuals presenting with similar clinical features are shown as filled black symbols (pedigrees are drawn to accepted standards[37]). A sequencing chromatogram obtained by targeted resequencing is shown for each proband, confirming the presence of the c.1555C>T (p.Gln519*) (S1), c.1303C>T (p.Arg435*) (S2), and c.1703G>CGC (S3) mutations.

observed in 1/13,005 chromosomes sequenced by the NHLBI Exome Sequencing Project. Familial segregation of the recessive mutations was clearly demonstrated (Figure 1).

FBXL4 Is a LRR F-Box Protein that Localizes to the Mitochondria

Computational analysis of the protein structure of FBXL4 revealed canonical features of a LRR F-box protein with a possible mitochondrial localization. Three-dimensional structural modeling and searches for conserved sequence domains elucidated the presence of the F-box and AMN1 domains in the C-terminal portion of the protein (Figures 2A and 2B). The second half of the protein containing the F-box and AMN1 domains (amino acids 280–600) showed 23% identity to SKP2. At least nine LRRs were clearly identified and an additional LRR may also exist although this could not be concluded with high confidence because of some disorder in the model. No conserved domains were identified in the N-terminal half of the protein. However, sequence analysis revealed a N-terminal mitochondrial localization signal (Figure 2A), the functionality of which was authenticated through immunolocalization studies that showed HA-tagged FBXL4 colocalizing with MitoTracker Red-labeled mitochondria (Figure 2D).

Skeletal Muscle and Fibroblasts from Individuals with *FBXL4* Mutations Show Combined Respiratory Chain Deficiencies

The index cases from all three families showed significant evidence of mitochondrial respiratory chain abnormalities in diagnostic muscle biopsies. Histological and histochemical analyses in S1 and S2 revealed evidence of respiratory chain deficiency, with decreased reactivity for COX histochemical activity in both cases (Figure 3A); in the example of S1, those fibers that show COX activity unusually have discrete, punctate activity in the sarcoplasm. Modified Gomori Trichrome staining revealed mild subsarcolemmal accumulations in both cases (data not shown), and the skeletal muscle biopsy of S3 revealed mild variation in fiber size, type 2 fiber predominance, a few fibers with slight increase in glycogen content, and occasional enlarged mitochondria on electron microscopy.

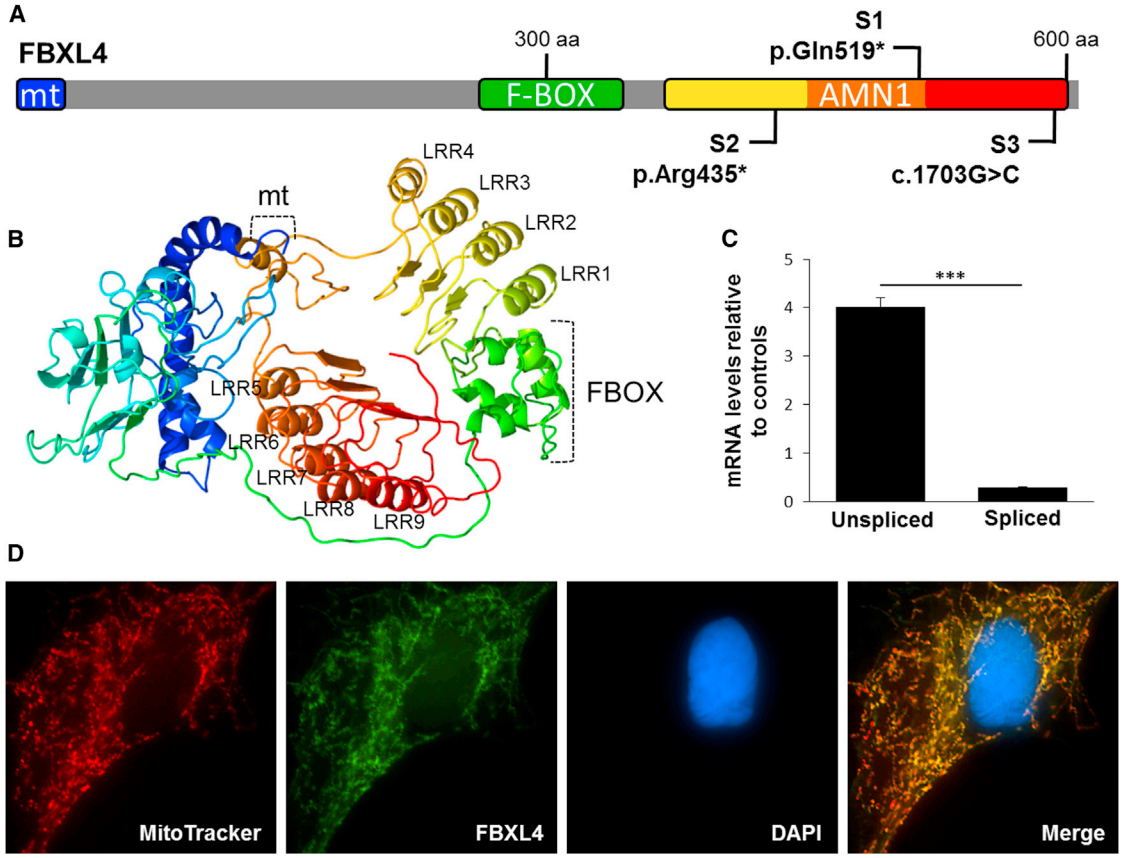

Figure 2. FBXL4 Protein Structure and Localization
(A) Schematic of FBXL4 showing the location of the bioinformatically determined mitochondrial localization sequence (mt) and conserved domains (F-box CDD ID pfam12937, AMN1 CDD ID cd09293). The locations of each of the mutations are indicated.
(B) Three-dimensional structural modeling of FBXL4 shows the canonical folds of the F-box and nine leucine-rich repeats. The protein schematic and 3D structure are both displayed in reverse rainbow from the N to C terminus.
(C) Splicing of exon 9 was demonstrated to be significantly impaired in S3 compared to controls. Error bars indicate standard deviation; ***$p < 0.0001$.
(D) FBXL4 was confirmed to be a mitochondrial protein through an immunolocalization study in human fibroblasts, showing HA-tagged FBXL4 (green) colocalizing with MitoTracker Red-labeled mitochondria. Nuclei were counterstained with DAPI (blue).

A profound, combined respiratory chain defect was confirmed in the muscle of S2 (Figure 3B), showing markedly decreased activities of complexes I, III, and IV with sparing of complex II activity. The biochemical defects were less pronounced in S1 and S3 although complex IV activity was ~60% of control values in both cases when related to citrate synthase activity (Figure 3B), a finding recapitulated in the direct measurement of respiratory chain complex activities in fibroblast cell lines (Figure 3C), which also all showed significantly ($p < 0.0001$) decreased mitochondrial membrane potential (Figure 3D). There was a suggestion that citrate synthase activity was decreased in the muscle from S1, thereby explaining why the relative OXPHOS activity defects were less pronounced and implying that *FBXL4* mutations may affect the activities of other mitochondrial enzymes apart from those containing mtDNA-encoded subunits (data not shown).

Microscale oxygraphy in fibroblasts from S1 (c.1555C>T [p.Gln519*]) and S2 (c.1303C>T [p.Arg435*]) provided additional evidence of a severe dysfunction of mitochondrial respiration (Figure 4A). Basal OCR and maximal OCR were both significantly reduced in S1 ($p = 0.0012$) and S2 ($p = 0.0005$). The reduced basal respiration in both individuals resulted in reduced synthesis of ATP by OXPHOS (Figure 4B) in comparison to controls ($p < 0.001$); to compensate for this loss, the amount of ATP produced by glycolysis (Figure 4B) in fibroblasts from affected individuals is increased ($p < 0.01$). The spare respiratory capacity of fibroblasts from S1 and S2 are significantly reduced in comparison to controls ($p < 0.0001$), suggesting that the mitochondria are working at near-maximal capacity, with little capability to respond to increased energy demand or stress (Figure 4C). The efficiency of the coupling of respiration and ATP synthesis was also significantly impaired in fibroblasts from S2 ($p < 0.0001$), indicating increased proton leak across the membrane (Figure 4D). Fibroblasts from S1 showed normal ATP coupling. Additionally, the steady-state levels of subunits from respiratory chain complexes containing

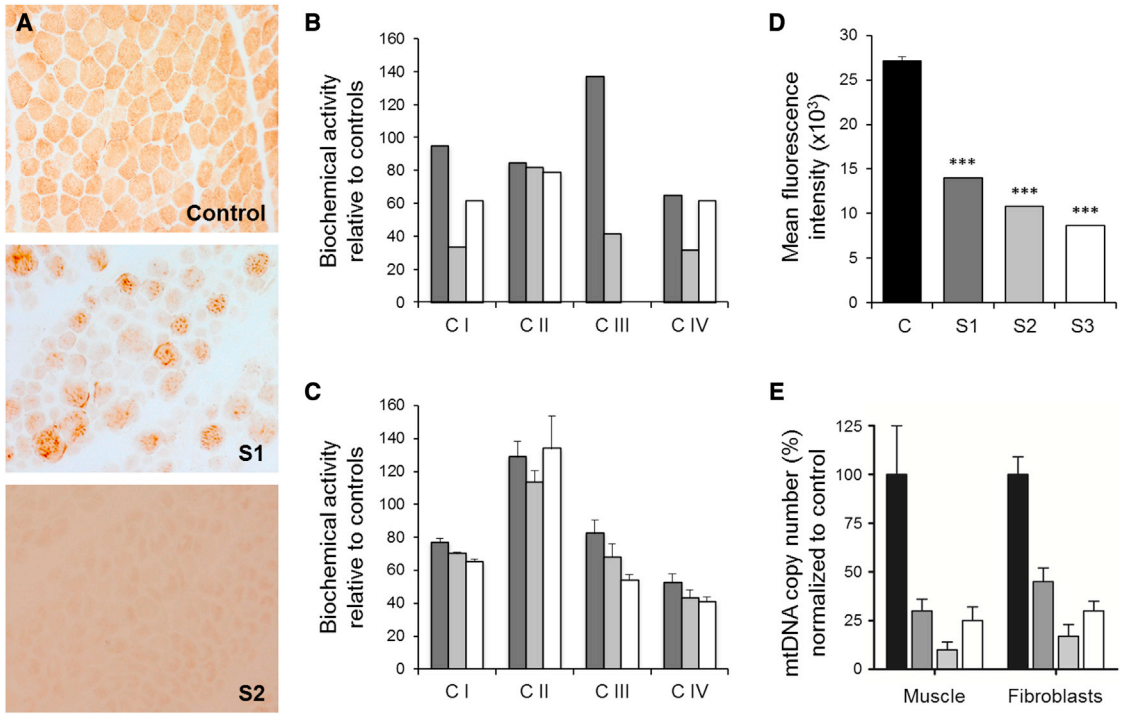

Figure 3. Individuals with *FBXL4* Mutations Display Mitochondrial Biochemical Dysfunction
(A) Cytochrome c oxidase (COX) histocytochemical activities in skeletal muscle from S1 and S2 are globally decreased in comparison to control muscle, although somewhat unusually there are occasional, COX-positive fibers in S1 showing discrete, punctate enzyme activity.
(B and C) Respiratory chain complex biochemical activity was determined in both skeletal muscle (B) and fibroblasts (C) from all probands (dark gray columns, S1; light gray columns, S2; white columns, S3) and is shown relative to the mean activity measured in 25 controls.
(D) Mitochondrial membrane potential was measured in fibroblasts from S1, S2, and S3 together with seven controls (C). Cells from each affected individual showed severely compromised membrane potential compared to controls. ***$p < 0.0001$.
(E) Severe depletion of mtDNA was determined in skeletal muscle and fibroblasts from each of the three probands (dark gray columns, S1; light gray columns, S2; white columns, S3) when measured in comparison to age-matched control muscle ($n = 20$) and fibroblasts ($n = 3$) (black columns).
For all data, error bars indicate standard deviation.

mtDNA-encoded subunits were found to be significantly decreased in fibroblasts from both S1 and S2 (Figure 4E), with the suggestion in S2 that expression of complex II subunits (SDHA) were affected; the severity of this loss of protein expression in the two fibroblast cell lines appear to reflect the location of the *FBXL4* truncating mutation. The mitochondrial marker TOMM20 was unchanged in patient fibroblasts, confirming normal mitochondrial protein content, thereby highlighting a specific problem with OXPHOS subunit biogenesis.

Skeletal Muscle and Fibroblasts from Individuals with *FBXL4* Mutations Show Severe mtDNA Depletion and Disruption of Mitochondrial Morphology

Analysis of mtDNA copy number (Figure 3E) in skeletal muscle by qPCR demonstrated severe mtDNA depletion in S1 (~30% of control), S2 (<10% of control), and S3 (25% of control), leading to the observed biochemical defects. This quantitative loss of mtDNA copy number was recapitulated in the fibroblasts (Figure 3E), with S1 (45% of control), S2 (17% of control), and S3 (30% of control) all showing evidence of mtDNA depletion.

We next investigated the mitochondrial morphology in cells to determine whether this was disturbed as documented in other mtDNA maintenance disorders. Assessment of the dynamic mitochondrial network and distribution of nucleoids in fibroblasts from both S1 and S2 revealed dramatic fragmentation and shortening of mitochondria when compared to controls (Figure 5, top). Nucleoids were enlarged and showed distinct perinuclear clustering in both cell lines compared to smaller more evenly distributed nucleoids within control cells (Figure 5, bottom).

Delivery of Wild-Type *FBXL4* to S1 and S2 Cells Rescues mtDNA Copy Number and Biochemical Defects

To verify that the mitochondrial respiratory chain defects and quantitative loss of mtDNA copy number observed in fibroblasts were due to loss of FBXL4 function, we conducted gene rescue experiments wherein either a wild-type copy of *FBXL4* or a negative control (*EGFP*) was virally delivered into cells from affected individuals (S1 and S2). Previous profiling of mitochondrial function

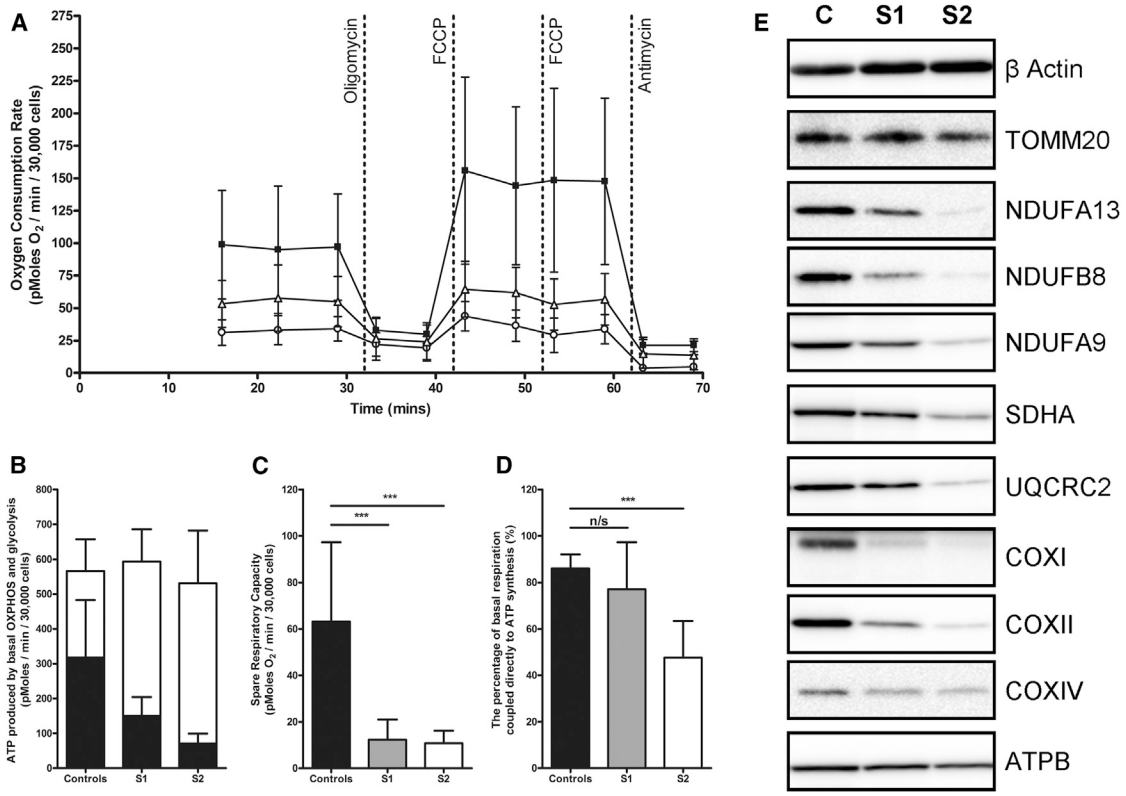

Figure 4. Characterization of the OXPHOS Defects in Fibroblasts

(A) Microscale oxygraphy analysis of live fibroblasts demonstrated a profound respiratory deficiency in cells from both S1 (c.1555C>T [p.Gln519*], n = 22, white triangles) and S2 (c.1303C>T [p.Arg435*], n = 14, white circles), compared to the combined data of control cell lines (n = 5, black squares). Error bars indicate the standard deviation.

(B) The total amount of ATP produced by fibroblasts from S1 and S2 is not dramatically different to controls, but the proportion contributed by OXPHOS (black columns) is significantly reduced, whereas that contributed by glycolysis (white columns) is significantly increased.

(C) The ability of fibroblasts from S1 and S2 to respond to stress, as measured by the spare respiratory capacity (maximal OCR minus basal OCR), is significantly reduced in comparison to controls. ***$p < 0.0001$.

(D) The efficiency of the coupling of respiration to ATP synthesis (oligomycin-sensitive OCR as a percent of basal OCR) was significantly impaired in fibroblasts from S2 but not S1 compared to controls. For all data, error bars indicate standard deviation. ***$p < 0.0001$; NS, not significant.

(E) Immunoblotting for protein components of each of the mitochondrial respiratory chain complexes was completed in S1 and S2 to determine their abundance relative to control (labeled C). Three subunits of complex I (NDUFA13, NDUFB8, and NDUFA9), one of complex II (SDHA), one of complex III (UQCRC2), three of complex IV (COXI, COXII, and COXIV), and one of complex V (ATPB) were probed, with TOMM20 as a mitochondrial marker and β-actin as a loading control.

in *FXBL4* mutant fibroblasts had identified decreased complex IV deficiency, membrane potential, and mtDNA depletion (Figures 3C–3E). S1 and S2 cells expressing *GFP* showed no significant improvement in these cellular phenotypes (Figures 6A–6C). In contrast, cells from both S1 and S2 expressing wild-type *FBXL4* demonstrated full rescue of mtDNA levels ($p < 0.0001$), complex IV biochemical activity ($p < 0.01$), and membrane potential ($p < 0.0001$) (Figures 6A–6C, respectively). In addition, control fibroblasts stably expressing *FBXL4* demonstrated that *FBXL4* mRNA levels similar to those in transformed cells from affected individuals (Figure 6D) showed no difference in mtDNA copy number or membrane potential, demonstrating that *FBXL4* overexpression itself does not cause an increase in mtDNA copy number or biochemical activity (Figure 6). These data provide unequivocal evidence that autosomal-recessive *FBXL4* mutations cause a quantitative loss of mtDNA copy number and associated OXPHOS activity defects in humans.

Discussion

We present the clinical, molecular, and functional investigation of multiple subjects from three unrelated families all of Arabian origin with combined OXPHOS deficiency resulting from severe mtDNA depletion. By combining whole-exome sequencing with profiling of mitochondrial function and gene rescue studies in cells from affected individuals, we identified and validated three independent, pathogenic alleles in the orphan F-box protein FBXL4 which, to our knowledge, has not previously been associated with human disease.

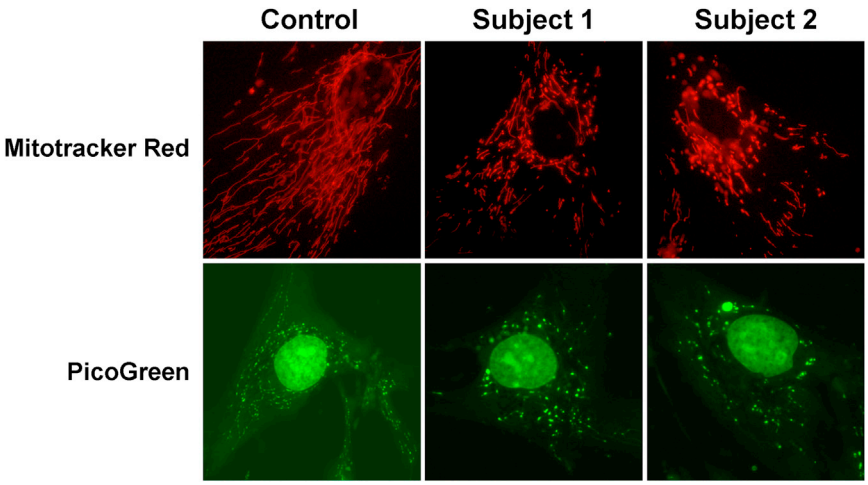

Figure 5. Mitochondrial Network and Nucleoid Morphology Is Disrupted in Individuals with *FBXL4* Mutations
The upper panels show representative images of MitoTracker Red staining of control (left), S1 (middle), and S2 (right) fibroblasts. Note fragmentation and shortening of mitochondria in both these cell lines compared to the control. The lower panels show nucleoid staining by PicoGreen, revealing larger nucleoids with perinuclear clustering in cells from both subjects.

We present overwhelming evidence in support of *FBXL4* mutations causing a severe respiratory chain deficiency resulting from dysregulation of mtDNA maintenance. Affected individuals with different *FBXL4* mutations display a highly overlapping clinical presentation with onset in the first years of life. Molecular analysis of tissues identified a common pattern of decreased mtDNA copy number and loss of mitochondrial membrane potential in cells. Furthermore, a severe mitochondrial respiratory deficiency was demonstrated in fibroblasts by microscale oxygraphy and immunoblotting of respiratory chain proteins. Key evidence supporting the pathogenic role of mutations in *FBXL4* was demonstrated through functional studies showing rescue of mtDNA copy number, biochemical activity, and membrane potential in cells from two affected individuals with different mutations transduced with wild-type *FBXL4*.

There are some notable differences among subjects' clinical and molecular phenotypes that are presumably linked to the severity of the causative *FBXL4* mutation. Both S1 and S2, who have nonsense mutations, died within the first 2 years of life. In contrast, S3, who has a missense mutation that affects splicing of the last exon, although severely affected with psychomotor retardation, was 6 years old at his last clinical evaluation and to our knowledge remains alive. In addition, functional evaluation showed evidence of a histocytochemical deficiency of COX in S1 and S2, whereas this was reported as normal in S3. Likewise, S2 has the most severe truncating mutation and was observed to show the most severe mtDNA depletion and most compromised mitochondrial respiratory chain activities in muscle.

The three families are linked by the common presentation of a disease phenotype consisting primarily of a fatal mitochondrial encephalopathy and lactic acidosis, which affected multiple members of each family in a pattern consistent with the homozygous recessive *FBXL4* mutations identified. Intrauterine growth retardation, microcephaly, and hypotonia were frequent nonspecific features in the affected children from the families but are not uncommon findings in mitochondrial disease. On the other hand, the craniofacial abnormalities, cataracts, and developmental brain abnormalities observed in several of these children are indicative of a specific disease phenotype associated with mutations in *FBXL4* and with onset at an early stage of fetal development. Classic myopathic, encephalomyopathic, and hepatocerebral presentations of mtDNA depletion syndromes are not typically associated with craniofacial or structural brain abnormalities, but early development of cataracts has been observed in individuals with reported mtDNA depletion resulting from mutations in acylglycerol kinase (*AGK* [MIM 610345]).[32] Interestingly, the mtDNA depletion associated with *AGK* mutations is thought to be indirect, secondary to an effect on phospholipid metabolism and adenine nucleotide transporter assembly in the inner mitochondrial membrane.[33] In the absence of an obvious role for FBXL4 in the mtDNA translation machinery, it is quite possible that a similarly circuitous mechanism is responsible for the mtDNA depletion observed in these cases.

FBXL4 is a member of a family of proteins that form a component of the Skp1-Cullin-F-box (SCF) ubiquitin ligase complex,[34] which has been shown to have role in phosphorylation-directed ubiquitination.[35,36] Although FBXL4 protein structure includes the canonical FBXL functional domains, as with other orphan F-box proteins, the precise function of this protein in human cells has not been described. Crucially, we have shown that *FBXL4* contains a mitochondrial localization signal and that the protein colocalizes with mitochondria. Furthermore, fibroblasts from S1 and S2 show dramatic disturbance of the mitochondrial network and significant redistribution of nucleoids in addition to mtDNA depletion. It seems likely that FBXL4 plays an important role in the maintenance of mtDNA, although an exact mechanism for this function remains undetermined. Further characterization of the specific mitochondrial sublocalization of FBXL4 and the interacting partners of this protein would begin to elucidate the mechanism by which *FBXL4* mutations exert their affect.

In conclusion, we report pathogenic mutations in *FBXL4* and demonstrate a role for the encoded orphan F-box protein in causing mitochondrial respiratory chain

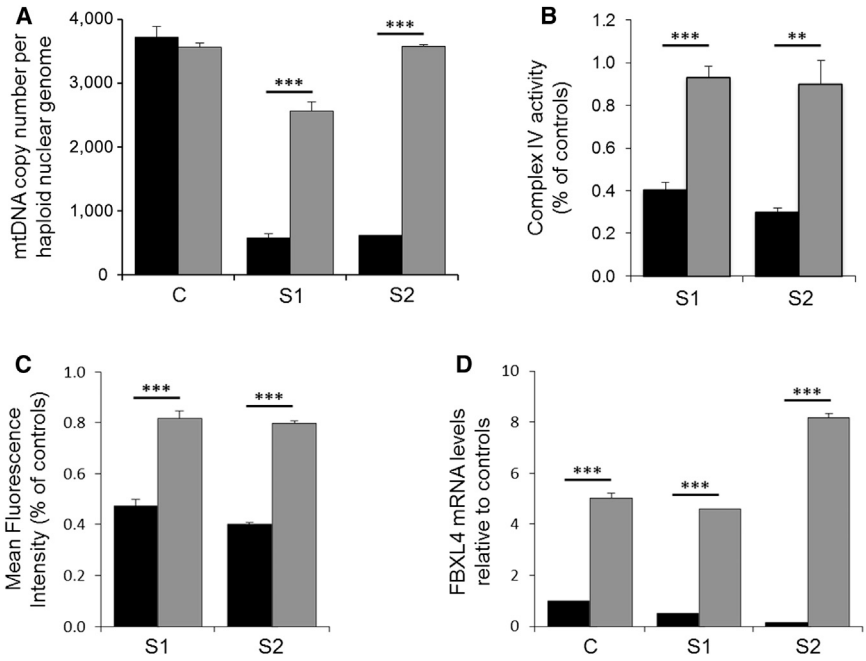

Figure 6. *FBXL4* Gene Rescue Studies in S1 and S2 Cells

Fibroblasts were transduced with either *GFP* (black columns) or wild-type *FBXL4* (gray columns) and compared to transduced control fibroblasts.

(A–C) mtDNA copy number (A), complex IV activity (B), and membrane potential (C) were recovered to normal levels in S1 and S2 fibroblasts transfected with wild-type FBXL4 but not GFP.

(D) FBXL4 mRNA levels were increased in control (C) and S1 and S2 fibroblasts infected with wild-type FBXL4 but not in those infected with *GFP*. Transcript levels are reported relative to *GAPDH*.

For all graphs, error bars indicate standard deviation; ***$p < 0.0001$, **$p < 0.01$.

deficiencies and depletion of mtDNA. Moreover, our study exemplifies the power of combining genome-wide sequencing with functional studies for the identification and verification of pathogenic mutations in human genes previously not associated with a disease phenotype.

Acknowledgments

This work was supported by the Texas Norman Hackerman Advanced Research Program under Grant No. [THECB] 02006, the Cytometry and Cell Sorting Core at Baylor College of Medicine with funding from the National Institutes of Health (AI036211, CA125123, and RR024574), NHARP proposal number 0049-0041-2009 (P.E.B.), a Medical Research Council (UK) Centenary Early Career Award (J.W.Y.), an HEFCE/DoH Clinical Senior Lecturer Award (R.M.), a Wellcome Trust Strategic Award (096919/Z/11/Z) (R.W.T.), the MRC Centre for Neuromuscular Diseases (G0601943) (R.M. and R.W.T.), the Lily Foundation (R.M. and R.W.T.), and the UK NHS Specialist Commissioners that funds the "Rare Mitochondrial Disorders of Adults and Children" Diagnostic Service in Newcastle upon Tyne. We thank the families for participating in this study and Gavin Falkous and Joel Sederstrom for excellent technical support.

Received: May 29, 2013
Revised: July 12, 2013
Accepted: July 17, 2013
Published: August 29, 2013

Web Resources

The URLs for data presented herein are as follows:

MitoProt, http://ihg.gsf.de/ihg/mitoprot.html
NCBI Conserved Domains, http://www.ncbi.nlm.nih.gov/Structure/cdd/wrpsb.cgi
Online Mendelian Inheritance in Man (OMIM), http://www.omim.org/
Phyre2, http://www.sbg.bio.ic.ac.uk/phyre2/html/page.cgi?id=index
UCSC Genome Browser, http://genome.ucsc.edu

References

1. Debray, F.G., Lambert, M., and Mitchell, G.A. (2008). Disorders of mitochondrial function. Curr. Opin. Pediatr. *20*, 471–482.
2. Koopman, W.J.H., Willems, P.H.G.M., and Smeitink, J.A.M. (2012). Monogenic mitochondrial disorders. N. Engl. J. Med. *366*, 1132–1141.
3. Pagliarini, D.J., Calvo, S.E., Chang, B., Sheth, S.A., Vafai, S.B., Ong, S.E., Walford, G.A., Sugiana, C., Boneh, A., Chen, W.K., et al. (2008). A mitochondrial protein compendium elucidates complex I disease biology. Cell *134*, 112–123.
4. Thorburn, D.R. (2004). Mitochondrial disorders: prevalence, myths and advances. J. Inherit. Metab. Dis. *27*, 349–362.
5. Pitceathly, R.D.S., Smith, C., Fratter, C., Alston, C.L., He, L.P., Craig, K., Blakely, E.L., Evans, J.C., Taylor, J., Shabbir, Z., et al. (2012). Adults with RRM2B-related mitochondrial disease have distinct clinical and molecular characteristics. Brain *135*, 3392–3403.
6. Suomalainen, A., and Isohanni, P. (2010). Mitochondrial DNA depletion syndromes—many genes, common mechanisms. Neuromuscul. Disord. *20*, 429–437.
7. Spinazzola, A., Viscomi, C., Fernandez-Vizarra, E., Carrara, F., D'Adamo, P., Calvo, S., Marsano, R.M., Donnini, C., Weiher, H., Strisciuglio, P., et al. (2006). MPV17 encodes an inner mitochondrial membrane protein and is mutated in infantile hepatic mitochondrial DNA depletion. Nat. Genet. *38*, 570–575.
8. Old, S.L., and Johnson, M.A. (1989). Methods of microphotometric assay of succinate dehydrogenase and cytochrome c

oxidase activities for use on human skeletal muscle. Histochem. J. *21*, 545–555.
9. Kirby, D.M., Thorburn, D.R., Turnbull, D.M., and Taylor, R.W. (2007). Biochemical assays of respiratory chain complex activity. Methods Cell Biol. *80*, 93–119.
10. Blakely, E.L., He, L., Taylor, R.W., Chinnery, P.F., Lightowlers, R.N., Schaefer, A.M., and Turnbull, D.M. (2004). Mitochondrial DNA deletion in "identical" twin brothers. J. Med. Genet. *41*, e19.
11. Taylor, R.W., Barron, M.J., Borthwick, G.M., Gospel, A., Chinnery, P.F., Samuels, D.C., Taylor, G.A., Plusa, S.M., Needham, S.J., Greaves, L.C., et al. (2003). Mitochondrial DNA mutations in human colonic crypt stem cells. J. Clin. Invest. *112*, 1351–1360.
12. Taylor, R.W., Taylor, G.A., Durham, S.E., and Turnbull, D.M. (2001). The determination of complete human mitochondrial DNA sequences in single cells: implications for the study of somatic mitochondrial DNA point mutations. Nucleic Acids Res. *29*, E74–E4.
13. Blakely, E., He, L., Gardner, J.L., Hudson, G., Walter, J., Hughes, I., Turnbull, D.M., and Taylor, R.W. (2008). Novel mutations in the TK2 gene associated with fatal mitochondrial DNA depletion myopathy. Neuromuscul. Disord. *18*, 557–560.
14. Bainbridge, M.N., Wang, M., Wu, Y., Newsham, I., Muzny, D.M., Jefferies, J.L., Albert, T.J., Burgess, D.L., and Gibbs, R.A. (2011). Targeted enrichment beyond the consensus coding DNA sequence exome reveals exons with higher variant densities. Genome Biol. *12*, R68.
15. Li, H., and Durbin, R. (2009). Fast and accurate short read alignment with Burrows-Wheeler transform. Bioinformatics *25*, 1754–1760.
16. DePristo, M.A., Banks, E., Poplin, R., Garimella, K.V., Maguire, J.R., Hartl, C., Philippakis, A.A., del Angel, G., Rivas, M.A., Hanna, M., et al. (2011). A framework for variation discovery and genotyping using next-generation DNA sequencing data. Nat. Genet. *43*, 491–498.
17. McKenna, A., Hanna, M., Banks, E., Sivachenko, A., Cibulskis, K., Kernytsky, A., Garimella, K., Altshuler, D., Gabriel, S., Daly, M., and DePristo, M.A. (2010). The Genome Analysis Toolkit: a MapReduce framework for analyzing next-generation DNA sequencing data. Genome Res. *20*, 1297–1303.
18. Ng, P.C., and Henikoff, S. (2001). Predicting deleterious amino acid substitutions. Genome Res. *11*, 863–874.
19. Adzhubei, I.A., Schmidt, S., Peshkin, L., Ramensky, V.E., Gerasimova, A., Bork, P., Kondrashov, A.S., and Sunyaev, S.R. (2010). A method and server for predicting damaging missense mutations. Nat. Methods *7*, 248–249.
20. Cooper, G.M., Stone, E.A., Asimenos, G., Green, E.D., Batzoglou, S., and Sidow, A.; NISC Comparative Sequencing Program. (2005). Distribution and intensity of constraint in mammalian genomic sequence. Genome Res. *15*, 901–913.
21. Davydov, E.V., Goode, D.L., Sirota, M., Cooper, G.M., Sidow, A., and Batzoglou, S. (2010). Identifying a high fraction of the human genome to be under selective constraint using GERP++. PLoS Comput. Biol. *6*, e1001025.
22. Siepel, A., Pollard, K.S., and Haussler, D. (2006). New methods for detecting lineage-specific selection. In Proceedings of the 10th International Conference on Research in Computational Molecular Biology. (RECOMB), pp. 190–205.
23. Wong, L.J., Perng, C.L., Hsu, C.H., Bai, R.K., Schelley, S., Vladutiu, G.D., Vogel, H., and Enns, G.M. (2003). Compensatory amplification of mtDNA in a patient with a novel deletion/duplication and high mutant load. J. Med. Genet. *40*, e125.
24. Bai, R.K., and Wong, L.J. (2005). Simultaneous detection and quantification of mitochondrial DNA deletion(s), depletion, and over-replication in patients with mitochondrial disease. J. Mol. Diagn. *7*, 613–622.
25. Kelley, L.A., and Sternberg, M.J. (2009). Protein structure prediction on the Web: a case study using the Phyre server. Nat. Protoc. *4*, 363–371.
26. Claros, M.G., and Vincens, P. (1996). Computational method to predict mitochondrially imported proteins and their targeting sequences. Eur. J. Biochem. *241*, 779–786.
27. Marchler-Bauer, A., Lu, S.N., Anderson, J.B., Chitsaz, F., Derbyshire, M.K., DeWeese-Scott, C., Fong, J.H., Geer, L.Y., Geer, R.C., Gonzales, N.R., et al. (2011). CDD: a Conserved Domain Database for the functional annotation of proteins. Nucleic Acids Res. *39*(Database issue), D225–D229.
28. Invernizzi, F., D'Amato, I., Jensen, P.B., Ravaglia, S., Zeviani, M., and Tiranti, V. (2012). Microscale oxygraphy reveals OXPHOS impairment in MRC mutant cells. Mitochondrion *12*, 328–335.
29. Brand, M.D., and Nicholls, D.G. (2011). Assessing mitochondrial dysfunction in cells. Biochem. J. *435*, 297–312.
30. Brand, M.D. (2005). The efficiency and plasticity of mitochondrial energy transduction. Biochem. Soc. Trans. *33*, 897–904.
31. Birket, M.J., Orr, A.L., Gerencser, A.A., Madden, D.T., Vitelli, C., Swistowski, A., Brand, M.D., and Zeng, X. (2011). A reduction in ATP demand and mitochondrial activity with neural differentiation of human embryonic stem cells. J. Cell Sci. *124*, 348–358.
32. Calvo, S.E., Compton, A.G., Hershman, S.G., Lim, S.C., Lieber, D.S., Tucker, E.J., Laskowski, A., Garone, C., Liu, S., Jaffe, D.B., et al. (2012). Molecular diagnosis of infantile mitochondrial disease with targeted next-generation sequencing. Sci. Transl. Med. *4*, 118ra110.
33. Mayr, J.A., Haack, T.B., Graf, E., Zimmermann, F.A., Wieland, T., Haberberger, B., Superti-Furga, A., Kirschner, J., Steinmann, B., Baumgartner, M.R., et al. (2012). Lack of the mitochondrial protein acylglycerol kinase causes Sengers syndrome. Am. J. Hum. Genet. *90*, 314–320.
34. Bai, C., Sen, P., Hofmann, K., Ma, L., Goebl, M., Harper, J.W., and Elledge, S.J. (1996). SKP1 connects cell cycle regulators to the ubiquitin proteolysis machinery through a novel motif, the F-box. Cell *86*, 263–274.
35. Cenciarelli, C., Chiaur, D.S., Guardavaccaro, D., Parks, W., Vidal, M., and Pagano, M. (1999). Identification of a family of human F-box proteins. Curr. Biol. *9*, 1177–1179.
36. Winston, J.T., Koepp, D.M., Zhu, C., Elledge, S.J., and Harper, J.W. (1999). A family of mammalian F-box proteins. Curr. Biol. *9*, 1180–1182.
37. Bennett, R.L., Steinhaus, K.A., Uhrich, S.B., O'Sullivan, C.K., Resta, R.G., Lochner-Doyle, D., Markel, D.S., Vincent, V., and Hamanishi, J.; Pedigree Standardization Task Force of the National Society of Genetic Counselors. (1995). Recommendations for standardized human pedigree nomenclature. Am. J. Hum. Genet. *56*, 745–752.